Journal Name

COMMUNICATION

Ni@onion-like carbon and Co@amorphous carbon: Control of carbon structures by metal ion species in MOFs

Received 00th January 20xx,
Accepted 00th January 20xx

DOI: 10.1039/x0xx00000x

www.rsc.org/

Megumi Mukoyoshi,[*a] Hirokazu Kobayashi,[a] Kohei Kusada,[a] Kazuya Otsubo,[a] Mitsuhiko Maesato,[a] Yoshiki Kubota,[b] Tomokazu Yamamoto,[c] Syo Matsumura[c, d] and Hiroshi Kitagawa[*a]

We first report the facile synthesis of metal–carbon composites consisting of metal nanoparticles (NPs) and different types of carbon species: onion-like and amorphous carbon, Ni@onion-like carbon and Co@amorphous carbon. By simply changing the metal species in an isostructural metal–organic framework, thermal decompositions of MOF-74 directly afforded different types of metal NPs and carbon composites, which exhibited good electrical conductivity. In particular, the Ni@onion-like carbon, having a well-ordered carbon structure, had high electrical conductivitiy (σ = 5.3 Ω^{-1} cm^{-1} at 295 K), explained by a modified model of the Efros–Shklovskii variable range hopping.

Metal–organic frameworks (MOFs)[1–3] have attracted increasing interest as precursors for preparing carbon materials with metal nanoparticles (NPs) via thermal decomposition.[4–8] MOFs can serve as precursors for both NPs and carbon materials; therefore, they can offer a facile synthesis method to control the size of NPs and the composition/structure of composites. MOF-derived carbon composites are reported to be promising materials in electrocatalysis and energy storage.[9-11] There are various types of carbon species, such as amorphous carbon, carbon nanotubes, and graphite. These species have different porosities, dimensions, and morphologies, which are related to properties such as gas storage, catalytic activity and conductivity. Control of the carbon structure and morphology is therefore significant.

To date, the focus of research on MOF-derived carbon composites has mainly been on the structure control of carbons based on the selection of the parent MOF structures and process conditions, such as the gas atmosphere, calcination temperature and post-treatment. For example, the surface area, pore volume, pore distribution and conductivity of carbons have been effectively controlled by using different types of the parent MOF structure.[6, 12] Furthermore, two different morphologies of carbon (nanofibers and nanocrystalline graphite) have been obtained by changing the gas atmosphere (air and N_2) during thermal decomposition of the MOF.[7] Recently, graphene nanoribbons were fabricated through relatively high temperature calcination (1000 °C) and KOH post-treatment.[8] However, to date, the control of carbon structures by means of different metal species constituting isostructural MOFs has not been investigated.

Here, we report on the synthesis of metal NPs and carbon composites with different carbon structures, achieved by

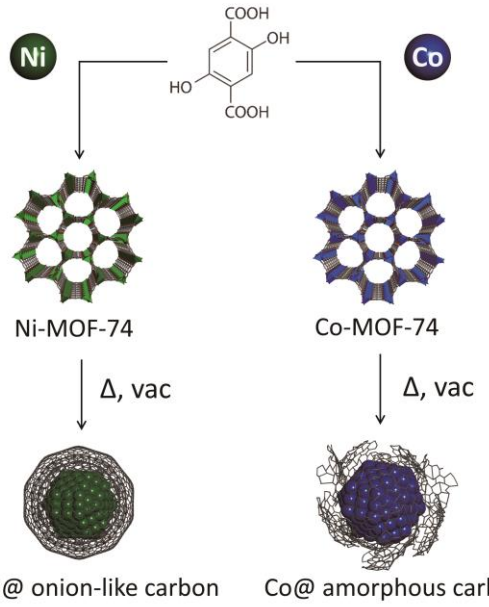

Scheme 1 Synthesis of Ni@onion-like carbon and Co @amorphous carbon.

[a] Division of Chemistry, Graduate School of Science, Kyoto University, Kitashirakawa-Oiwakecho, Sakyo-ku, Kyoto 606-8502, Japan
[b] Department of Physical Science, Graduate School of Science, Osaka Prefecture University, 1-1 Gakuen-cho, Sakai, Osaka 599-8531, Japan
[c] The Ultramicroscopy Research Center, Kyushu University, Motooka 744, Nishi-ku, Fukuoka 819-0395, Japan
[d] Department of Applied Quantum Physics and Nuclear Engineering, Graduate School of Engineering, Kyushu University, Motooka 744, Nishi-ku, Fukuoka 819-0395, Japan

† Electronic Supplementary Information (ESI) available: Experimental details, TG analysis, heat treatment, X-ray diffraction, TEM images, Raman spectra and Nitrogen sorption. See DOI: 10.1039/x0xx00000x

changing the metal ion in MOF-74, M_2(dhtp) (M = Ni, Co, H_4dhtp = 2,5-dihydroxyterephthalic acid). Thermal decomposition of the MOFs afforded Ni@onion-like carbon and Co@amorphous carbon (Scheme 1).

To obtain these carbon composites, we used MOF-74, which possesses a large cylindrical one-dimensional pore (diameter 11 Å).[13] MOF-74 consists of a combination of a metal ion and a functionalized hydroquinone ligand, which may act as a reducing agent for a metal ion. Ni-MOF-74 and Co-MOF-74 were synthesized using a slightly modified procedure reported earlier (see the ESI†).[14] Sample quality was determined by using thermogravimetric analysis (TGA) and powder X-ray diffraction (PXRD). TGA revealed that the decompositions of Ni-MOF-74 and Co-MOF-74 occur in the temperature ranges 350–410 and 420–500 °C, respectively (Fig. S1†). Ni-MOF-74 and Co-MOF-74 were then heated to 400 or 430 °C and held for 12 or 24 h under vacuum. Fig. 1a shows the PXRD patterns of Ni-MOF-74 and Ni-MOF-74 heated at 400 °C for 12 h under vacuum (**Ni 400-12h**). **Ni 400-12h** showed no diffraction pattern of Ni-MOF-74; only a face-centred cubic (fcc) Ni diffraction peaks were observed, as reported in our previous study.[15] Using the Le Bail method, a lattice constant of the fcc Ni was calculated to be a = 3.5190(3) Å; this is consistent with a value for bulk fcc Ni (3.524 Å).[16] The estimated crystal size was 6.199(17) nm (Fig. S2a†). Fig. 1b shows the PXRD patterns of Co-MOF-74, Co-MOF-74 heated at 400 °C for 12 h (**Co 400-12h**) and at 430 °C for 24 h (**Co 430-24h**). In the case of **Co 400-12h**, broad peaks corresponding to a fcc lattice were observed along with the Co-MOF-74 pattern, showing that the thermal decomposition of Co-MOF-74 was incomplete. Therefore, in an effort to achieve complete thermal decomposition, we used a higher temperature treatment and longer decomposition time.

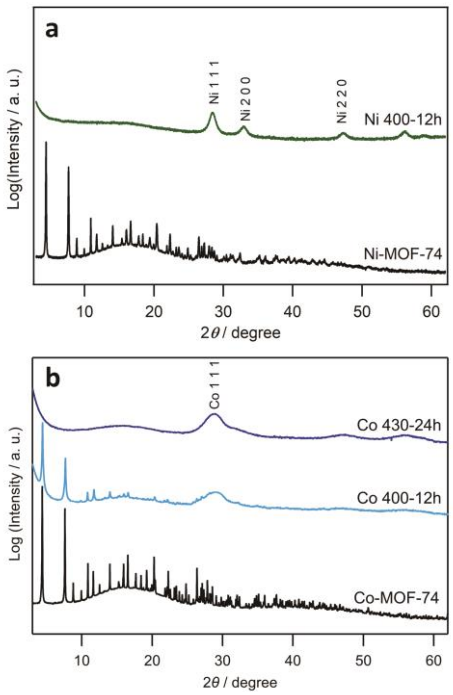

Fig. 1 (a) Synchrotron PXRD patterns of Ni-MOF-74 (black line) and **Ni 400-12h** (green line). Radiation wavelength 0.998 Å.(b) Synchrotron PXRD patterns of Co-MOF-74 (black line), **Co 400-12h** (light blue line) and **Co 430-24h** (blue line). Radiation wavelength 1.000 Å. For both (a) and (b), the y-axis is a logarithmic scale.

Subsequently, **Co 430-24h** showed no diffraction pattern of Co-MOF-74, thus indicating that complete decomposition of the initial Co-MOF-74 had taken place. These results were consistent with the TGA measurements, which indicated that, for complete decomposition, Co-MOF-74 requires higher temperature treatment than Ni-MOF-74 (Fig. S1†). Bulk Co is known to have a hexagonal close-packed (hcp) structure as the most stable phase at room temperature, but a fcc structure can often be obtained by reducing the particle size.[17] However, using the Le Bail fitting, an a = 3.5911(96) Å lattice constant was obtained. This value is slightly larger than for fcc Co (3.544 Å).[18] The increased lattice constant is considered to be a carbon supersaturated phase of the fcc Co (Co–C). Although carbon hardly forms a solid solution with Co at room temperature according to the phase diagram of Co–C,[19] it is well known that a supersaturated solid solution is formed by liquid quenching at high temperature[20] or by mechanical alloying.[21] The carbon content in Co–C can be estimated from the lattice constant a, by using the relationship a = 3.5447 + 0.0063 × (at%) Å.[21] The amount of dissolved carbon in **Co 430-24h** was estimated to be 7.4 at%. The estimated crystal size was 1.9 nm (Fig. S2b†). The difference in the generated NPs (Ni and Co–C) could be attributed to the differences in affinities of Ni and Co for carbon; Co forms stronger bonds with C than Ni does and interacts with C more readily. [22]

Fig. 2a shows a high-resolution scanning transmission electron microscopy (HR-STEM) image of **Ni 400-12h**. Ni NPs were distributed throughout the carbon matrices. The mean diameter of NPs was estimated to be 4.5 ± 1.2 nm, which is consistent with the crystal size calculated from the PXRD data (6.2 nm). Fig. 2b shows an onion-like carbon; multiple-shell spheres consisting of graphite sheets are evident.[23] From the HRSTEM image, the inter-shell distance was estimated to be 0.34 nm, which is consistent with the (002) lattice plane of graphite.[24] HRSTEM images taken at different tilting angles demonstrated that **Ni 400-12h** consists of Ni NPs covered with carbon (Fig. S3†). On the other hand, in **Co 430-24h**, the mean diameter of Co NPs was estimated to be 3.7 ± 0.7 nm, which is almost consistent with the crystal size calculated from the PXRD data (1.9 nm). It is noteworthy that, here, concentric multiple graphite sheets were not observed; alternatively, disordered graphitic layers were formed on Co NPs (Fig. 2c, d). These results strongly suggest that different carbon species are obtained from MOF-74 with different metal ions.

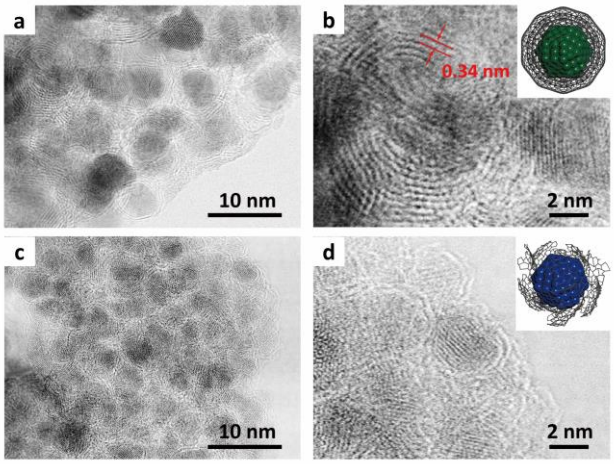

Fig. 2 HR-STEM images: (a) and (b) **Ni 400-12h**; (c) and (d) **Co 430-24h**.

Fig. 3 shows the Raman spectra of **Ni 400-12h**, **Co 430-24h**, Ni-MOF-74 and Co-MOF-74. After the thermal decomposition, the Raman bands of the dhtp ligand centred at 1618, 1560, 1499, 1414 and 1273 cm^{-1} for MOF-74[25] disappeared, whereas two broad bands centred at 1345 and 1587 cm^{-1} appeared. The latter are attributed to the D and G bands of carbon, respectively. These D and G bands are associated with disordered carbon and vibrations from entirely sp^2-bonded carbons, respectively.[26] For the Raman spectrum of **Co 430-24h**, only D and G bands were observed, as is the case with **Ni**

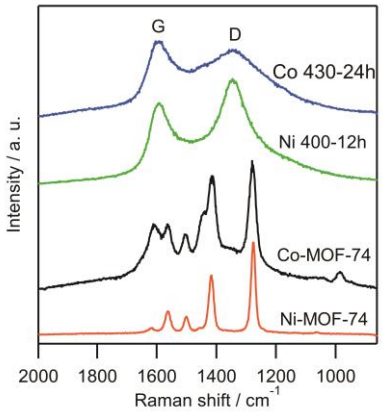

Fig. 3 Raman spectra of Ni-MOF-74 (orange line), Co-MOF-74(black line), **Ni 400-12h** (green line) and **Co 430-24h** (blue line).

400-12h. However, the integrated intensity ratio of D and G bands, tand the D band width, differed from those of **Ni 400-12h**, suggesting that different carbon species were generated, depending on the metal ions (Ni^{2+} or Co^{2+}) in MOF-74. The increases in integrated intensity ratio (I_D/I_G) and the D band width in **Co 430-24h**, compared with in **Ni 400-12h** (Table S2†) , indicate that **Co 430-24h** has a more disordered structure than **Ni 400-12h**.[27] These results are consistent with the results suggested from HRSTEM images, that is, different carbon species of onion-like carbon and disordered amorphous carbon were obtained.

N_2 adsorption/desorption isotherms were measured at 77 K to confirm the porosity of MOF-74 and MOF-derived carbon composites (Fig. S6†). Ni-MOF-74 and Co-MOF-74 showed the type I isotherm shape with a steep uptake at very low pressure, due to micropore filling.[28] The values of the specific Brunauer–Emmett–Teller (BET) surface areas (S_{BET}) of Ni-MOF-74 and Co-MOF-74 were almost the same as those reported previously.[29, 30] The isotherm of **Ni 400-12h** was classified as type II, characteristic of non-porous materials.[28] This result is consistent with the isotherm of onion-like carbon.[31] In contrast, **Co 400-24h** exhibited a type IV isotherm, with a H2 hysteresis loop. The adsorption/desorption hysteresis at >0.6 P/P_0, at which capillary gas condensation occurs, indicates the existence of mesopores.[28] These results suggest the difference in carbon structure between **Ni 400-12h** and **Co 430-24h**, that is, **Ni 400-12h** has a more ordered structure. The specific surface areas of **Ni 400-12h** and **Co 430-24h** were calculated to be S_{BET} = 165.1 and 263.3 m^2/g, respectively (Table S3†).

As shown in Fig. 5a, **Ni 400-12h** exhibits a high electrical conductivity (σ = 5.3 Ω^{-1} cm^{-1} at 295 K) because the graphitized carbon surrounds the Ni NPs. This conductivity is in the same range as the reported value for the onion-like carbon.[32] It has been reported that onion-like carbon shows higher electrochemical performance in supercapacitors than other carbon materials.[33] The electrical conductivity of **Co 430-24h** was recorded as 9.1×10^{-2} Ω^{-1} cm^{-1} at 295 K, which is somewhat similar to the case of the amorphous carbon ($\sigma < 1$ Ω^{-1} cm^{-1}).[34] In both samples, the electrical resistivity (ρ) gradually increased with decreasing temperature, indicating semiconducting behaviour. The charge transport property of **Co 430-24h** shows simple Arrhenius behaviour with activation energy E_a = 28.3 meV, that is, ln $\rho \sim T^{-1}$ (Fig. 4c), which implies that the conductivity is dominated by the amorphous carbon of **Co 430-24h**. On the other hand, in **Ni 400-12h**, the increase in resistivity does not follow the Arrhenius law. Instead, the behaviour can be explained by a modified model of the Efros–Shklovskii variable range hopping with $T^{-2/3}$ dependence (Fig. 4b), which is often observed when assembling NPs.[35]

Methods for fabricating onion-like carbon generally require high temperatures (>1400 °C)[32] or extreme conditions, such as arc discharge and electron irradiation.[23] In this study, we found that the carbon can be synthesized at temperatures as low as only 400 °C. We also found that the different carbon species can be synthesized by changing metal ions, using isostructural MOFs. This could originate from the difference in lattice constants of Ni and Co–C. It has been reported that graphene growth is more likely to occur if the graphene honeycomb lattice matches the lattice of the metal surface.[36] The lattice constant of a Ni(111) surface is similar to that of graphene (lattice mismatch 1.2%).[37] During the thermal decomposition of Ni-MOF-74, carbon derived from an organic ligand could interact with Ni NPs and transform into multiple graphitic sheets. In the case of **Co 430-24h**, due to a relatively larger lattice mismatch of Co–C (3.3%) compared with that of Ni, the transformation may not take place. This may be the reason why Co-MOF-74 resulted in amorphous carbon, produced by the initial thermal decomposition of MOF.

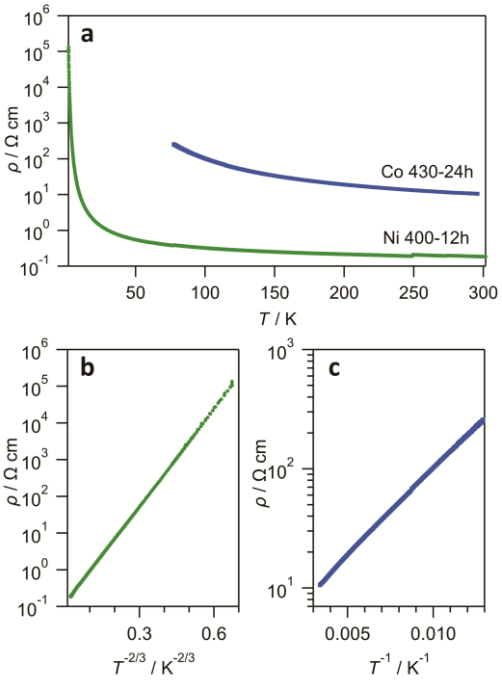

Fig. 4 (a) Electrical resistivity of **Ni 400-12h** and **Co-430-24h**. (b)$T^{-2/3}$ plot of the electrical resistivity of **Ni 400-12h**. (c) T^{-1} plot of the electrical resistivity of **Co 430-24h**.

In summary, we have demonstrated a facile synthesis of two different metal@carbon composites by simply changing the metal species in an isostructural MOF. HRSTEM images revealed the existence of different carbon species, in each of the composites: onion-like carbon and amorphous carbon. Raman spectra and N_2 adsorption/desorption isotherms supported the structural difference between these two composites; Ni@onion-like carbon has a more well-ordered structure than Co@amorphous carbon. It is notable that onion-like carbon can be synthesized at a relatively low temperature. These composites exhibited different conducting properties, due to their different structures. This approach should be very useful in the future design of various MOF-based nanoparticle composites with carbon, for nanostructured functional materials.

This work was supported by Core Research for Evolutional Science and Technology (CREST) 'Creation of Innovative Functions of Intelligent Materials on the Basis of the Element Strategy', ACCEL from Japan Science and Technology Agency (JST), and Grant-in-Aid for Specially Promoted Research (20H05623). STEM observations were performed as part of a program conducted by the Advanced Characterization Nanotechnology Platform sponsored by the Ministry of Education, Culture, Sports, Science and Technology (MEXT) of the Japanese government. Synchrotron XRD measurements were performed at SPring-8, supported by the Japan Synchrotron Radiation Research Institute (JASRI) (Proposal No. 2012A1503, 2012B1508, 2013A1473 and 2013B1403).

Conflicts of interest

There are no conflicts to declare.

Notes and references

1 S. Kitagawa, R. Kitaura and S. Noro, *Angew. Chem., Int. Ed.*, 2004, **43**, 2334–75.
2 J. R. Long and O. M. Yaghi, *Chem. Soc. Rev.*, 2009, **38**, 1213–1214.
3 O. M. Yaghi, M. O'Keeffe, N. W. Ockwig, H. K. Chae, M. Eddaoudi and J. Kim, *Nature*, 2003, **423**, 705–714.
4 B. Liu, H. Shioyama, T. Akita and Q. Xu, *J. Am. Chem. Soc.*, 2008, **130**, 5390–5391.
5 S. Chen, M. Xue, Y. Li, Y. Pan, L. Zhu and S. Qiu, *J. Mater. Chem. A*, 2015, **3**, 20145–20152.
6 G. Srinivas, V. Krungleviciute, Z. X. Guo and T. Yildirim, *Energy Environ. Sci.*, 2014, **7**, 335–342.
7 R. Das, P. Pachfule, R. Banerjee and P. Poddar, *Nanoscale*, 2012, **4**, 591–599.
8 P. Pachfule, D. Shinde, M. Majumder and Q. Xu, *Nat. Chem.*, 2016, **8**, 718–724.
9 Y. Yang, M. L. Li, J. N. Lin, M. Y. Zou, S. T. Gu, X. J. Hong, L. P. Si and Y. P. Cai, *Inorg. Chem.*, 2020, **59**, 2406–2412.
10 J. Jin, W. Cai, J. Cai, Y. Shao, Y. Song, Z. Xia, Q. Zhang and J. Sun, *J. Mater. Chem. A*, 2020, **8**, 3027–3034.
11 L. Meng, L. Zhang, Y. Zhu, H. Jiang, Y. V. Kaneti, J. Na, Y. Yamauchi, D. Golberg, H. Jiang and C. Li, *Nanoscale*, 2021, **13**, 1213–1219.
12 P. Pachfule, B. P. Biswal and R. Banerjee, *Chem. - A Eur. J.*, 2012, **18**, 11399–11408.
13 P. D. C. Dietzel, B. Panella, M. Hirscher, R. Blom and H. Fjellvåg, *Chem. Commun.*, 2006, **1**, 959–61.
14 S. R. Caskey, A. G. Wong-Foy and A. J. Matzger, *J. Am. Chem. Soc.*, 2008, **130**, 10870–1.
15 M. Mukoyoshi, H. Kobayashi, K. Kusada, M. Hayashi, T. Yamada, M. Maesato, J. M. Taylor, Y. Kubota, K. Kato, M. Takata, T. Yamamoto, S. Matsumura and H. Kitagawa, *Chem. Commun.*, 2015, **51**, 12463–12466.
16 H. Chessin, S. Arajs and R. Colvin, *J. Appl. Phys.*, 1964, **35**, 2419–2423.
17 O. Kitakami, H. Sato, Y. Shimada, F. Sato and M. Tanaka, *Phys. Rev. B - Condens. Matter Mater. Phys.*, 1997, **56**, 13849–13854.
18 A. Taylor and R. W. Floyd, *Acta Crystallogr.*, 1950, **3**, 285–289.
19 K.Ishida and T. Nishizawa, *J. Phase Equilib.*, 1991, **12**, 417–424.
20 R. C. Ruhl and M. Cohen, *Scr. Metall.*, 1967, **1**, 73–74.
21 T. Tanaka, K. N. Ishihara and P. H. Shingu, *Metall. Trans. A*, 1992, **23**, 2431–2435.
22 A. Õya and H. Marsh, *J. Mater. Sci.*, 1982, **17**, 309–322.
23 D. Urgate, *Nature*, 1992, **359**, 707–709.
24 C. He, N. Zhao, X. Du, C. Shi, J. Ding, J. Li and Y. Li, *Scr. Mater.*, 2006, **54**, 689–693.
25 L. Valenzano, J. G. Vitillo, S. Chavan, B. Civalleri, F. Bonino, S. Bordiga and C. Lamberti, *Catal. Today*, 2012, **182**, 67–79.
26 F. Tunistra and J. L. Koening, *J. Chem. Phys.*, 1970, **53**, 1126–1130.
27 K. Bogdanov, A. Fedorov, V. Osipov, T. Enoki, K. Takai, T. Hayashi, V. Ermakov, S. Moshkalev and A. Baranov, *Carbon*, 2014, **73**, 78–86.
28 M. Thommes, K. Kaneko, A. V. Neimark, J. P. Olivier, F. Rodriguez-Reinoso, J. Rouquerol and K. S. W. Sing, *Pure Appl. Chem.*, 2015, **87**, 1051–1069.
29 H. Oh, S. Maurer, R. Balderas-Xicohtencatl, L. Arnold, O. V. Magdysyuk, G. Schütz, U. Müller and M. Hirscher, *Int. J. Hydrogen Energy*, 2017, **42**, 1027–1035.
30 H. Y. Cho, D. A. Yang, J. Kim, S. Y. Jeong and W. S. Ahn, *Catal. Today*, 2012, **185**, 35–40.
31 G. Moussa, C. M. Ghimbeu, P. L. Taberna, P. Simon and C. Vix-Guterl, *Carbon*, 2016, **105**, 628–637.
32 V. L. Kuznetsov, Y. V. Butenko, A. L. Chuvilin, A. I. Romanenko and A. V. Okotrub, *Chem. Phys. Lett.*, 2001, **336**, 397–404.
33 D. Pech, M. Brunet, H. Durou, P. Huang, V. Mochalin, Y. Gogotsi, P. L. Taberna and P. Simon, *Nat. Nanotechnol.*, 2010, **5**, 651–654.
34 S. H. Moustafa, M. Koós and I. Pócsik, *J. Non-Cryst. Solids*, 1998, **227**–**230**, 1087–1091.
35 A. J. Houtepen, D. Kockmann and D. Vanmaekelbergh, *Nano Lett.*, 2008, **8**, 3516–3520.
36 H. Tetlow, J. Posthuma de Boer, I. J. Ford, D. D. Vvedensky, J. Coraux and L. Kantorovich, *Phys. Rep.*, 2014, **542**, 195–295.
37 P. A. Khomyakov, G. Giovannetti, P. C. Rusu, G. Brocks, J. van den Brink and P. J. Kelly, *Phys. Rev. B*, 2009, **79**, 1–12.

